

# MmWave vehicle-to-infrastructure communication: Analysis of urban microcellular networks

Yuyang Wang, Kiran Venugopal, Andreas F. Molisch, Robert W. Heath Jr.

**Abstract**—Vehicle-to-infrastructure (V2I) communication may provide high data rates to vehicles via millimeter-wave (mmWave) microcellular networks. This paper uses stochastic geometry to analyze the coverage of urban mmWave microcellular networks. Prior work used a pathloss model with a line-of-sight probability function based on randomly oriented buildings, to determine whether a link was line-of-sight or non-line-of-sight. In this paper, we use a pathloss model inspired by measurements, which uses a Manhattan distance model and accounts for differences in pathloss exponents and losses when turning corners. In our model, users and base stations (BSs) are randomly located on a network formed by a two dimensional Poisson line process. Our model is well suited for urban microcellular networks where the base stations are deployed at street level. Based on this new approach, we derive the coverage probability under certain BS association rules to obtain closed-form solutions without much complexity. In addition, we draw two main conclusions from our work. First, non-line-of-sight BSs are not a major benefit for association or source of interference. Second, there is an ultra-dense regime where deploying (active) BSs does not enhance coverage.

## I. INTRODUCTION

Vehicle-to-infrastructure (V2I) communication offers the potential to enhance safety and efficiency in urban vehicular networks [2–4]. Combined with millimeter wave (mmWave) [5–7], V2I has the potential to offer high data rates and low latency [8–10], to enable massive data sharing among a great number and diversity of mobile devices in vehicular networks [8, 11]. MmWave communication not only has access to larger bandwidths, it can also allow compact yet very large antenna arrays at both the transmitter and receiver to provide high directional beamforming gains and low interference. Compared to channels at cellular frequencies (<6 GHz), however, mmWave channels are more sensitive to blockage losses, especially in the urban streets where signals are blocked by high buildings, vehicles or pedestrians [10], [12], and sharp transitions from line-of-sight (LOS) to non-line-of-sight

(NLOS) links are more common<sup>1</sup>. This motivates the study of mmWave microcellular networks performance in the context of vehicular urban areas.

### A. Related Work

**Stochastic geometry** Stochastic geometry has been used extensively to analyze performance in mmWave cellular networks [13–18]. BS and cellular user locations are modeled as Poisson point processes on a two-dimensional plane, based on which the coverage probability of a *typical* cellular user is derived. Also, building blockages are considered as the main source differentiating LOS and NLOS links, with a few papers analyzing different building blockage models. Unfortunately, prior work analyzing mmWave cellular networks in [13–18] employed a pathloss model with a LOS probability function based on Euclidean distance [19], to determine whether a link was LOS or NLOS. This works well for randomly oriented buildings [14], but does not properly model V2I networks where strong LOS interference may result from infrastructure co-located on the same street.

Recent work has considered alternative topologies that may better model urban areas. In [20], an approach to determine LOS and NLOS BSs by approximating a *LOS ball* was proposed. The model was shown to be able to better approximate the LOS area than [19]. In [21], three-dimensional Poisson buildings were modeled using Poisson processes to characterize the correlated shadowing effects in urban buildings. The idea was to add one more dimension to the Manhattan Poisson line processes (MPLP), by modeling the floor locations as Poisson process. This allowed an exact characterization of coverage of in-door urban cellular networks. In [15], a stochastic geometry model in a Manhattan type network was analyzed, since it is a tractable yet realistic model for Manhattan type urban streets. The urban streets were modeled as one-dimensional MPLP and the coverage probability was derived considering the penetration effects of buildings. Unfortunately, the results in [15] using a pathloss model mainly considering the penetration effects of signals through urban buildings, with a fixed loss for each penetration. This is not applicable for mmWave systems where penetration loss is high. We also

Yuyang Wang, Kiran Venugopal and Robert W. Heath Jr. are with the Department of Electrical and Computer Engineering, the University of Texas at Austin, Austin, TX, 78712 USA, email: {yuywang, kiranv, rheath}@utexas.edu.

Andreas F. Molisch is with the Department of Electrical Engineering, University of Southern California, Los Angeles, CA, 90089-2565 USA, email: {molisch}@usc.edu.

Part of this work has been presented in IEEE VTC fall 2016 [1]. This research was partially supported by the U.S. Department of Transportation through the Data-Supported Transportation Operations and Planning (D-STOP) Tier 1 University Transportation Center, and by the Texas Department of Transportation under Project 0-6877 entitled “Communications and Radar-Supported Transportation Operations and Planning (CAR-STOP)”. The work of A. F. Molisch was supported by the National Science Foundation and a gift from Samsung.

<sup>1</sup>While in the propagation literature, including the papers cited here, LOS is defined as “optical” line of sight between the transmitter and receiver *location*. In the current paper, LOS link is defined here for the beamforming case, namely, as the case when both transmitter and receiver antennas are pointing towards each other without obstructions and having their azimuth and elevation planes aligned. NLOS link happens when 1) the link between the transmitter and the receiver is blocked by obstructions; 2) antennas of the transmitter and the receiver are not pointing to each other or are not properly aligned.

use the MPLP for modeling the urban street distribution, but combined with a mmWave-specific channel model.

**Urban mmWave channel modeling** There is a vast body of literature concerning mmWave channel modeling in urban areas, see, e.g., [22] and references therein. One of the key characteristics of urban environment is the high density of streets and high-rise buildings. Since mmWave signals are very sensitive to blockage, which induces significant signal attenuation, LOS and NLOS links can have sharply different pathloss exponents, as was also shown in numerous measurements [6][23][24], and is reflected in the standardized channel models [25]. Investigations in a variety of environments showed that in general, penetration loss increases with carrier frequency. For modern buildings with steel concrete and energy saving windows, in particular, penetration through just one wall can incur losses on the order of 30 dB; therefore propagation *through* buildings is not a relevant effect in mmWave urban environments [26].

In [27], a spatially consistent pathloss model was proposed for urban mmWave channels in microcells. Based on ray tracing, it was shown that the pathloss exponents differ from street to street and should be modeled as a function of both the street orientation and the absolute location of the BS and user equipment (UE)<sup>2</sup>. Hence, the signal is seen as propagating along different streets, with diffraction effects happening at the corner, instead of penetrating through the urban buildings. The pathloss is summed up by the individual pathloss on different segments of the propagation paths, incorporating an additional loss at each corner. This shows that the Euclidean distance might not be a good measure to characterize the pathloss effects in urban microcell networks at mmWave. In this paper, we adopt a modified pathloss model similar to [27] based on the Manhattan distance, which enables tractable analysis while still retaining the key features of the model.

### B. Contributions

In this paper, we develop a tractable framework to characterize the downlink coverage performance of urban mmWave microcells. We model the location of urban streets by a MPLP. The width of the street is neglected, and herein the blockage effects of vehicles are not considered in the analysis. We extend our previous paper [1] to account for large antenna arrays and directional beamforming at mmWave. We use a modification of the sectorized antenna model for tractable analysis [14, 28] and apply the new pathloss model from [27]. The pathloss model is characterized by the Manhattan distance of the propagation link, which, with MPLP street modeling, yields tractable results for coverage analysis.

Based on our model, we analyze coverage of randomly located UEs on the roads formed by the lines, which is different from the conventional approach where coverage is analyzed conditioned on the links being outdoors [14]. We adopt a new procedure in the calculation of coverage probability, compared to the previous work [14]. We analyze the coverage probability by first computing the cumulative

distribution function (CDF) of association link gain and then the coverage probability conditioned on the associated link gain. By averaging over the conditioned channel gain, we obtain simple but exact expression of coverage probability. We also examine the probability that the link is LOS. In addition, we fit our pathloss and street models to Euclidean distance based pathloss models for comparison. The results show significant differences, thus justifying the microcellular analysis using the Manhattan distance pathloss model.

Compared to [1], this paper also includes the following contributions. Based on the coverage probability, we obtain useful insights concerning the scaling laws of coverage probability with street and BS intensities, the sensitivity to propagation environment changes of LOS/NLOS paths and the effects of LOS/NLOS interference. Also, we derive closed-form expression of the LOS BS association probability. We then use the data of real streets in downtown Chicago from *OpenStreetMap* [29–31] and extract it using Geographical Information System (GIS) application *QGIS* [32]. This is used to compare the ergodic rate of realistic streets, MPLP street model and fixed grid models, and MPLP-based analysis is validated for an outdoor microcell urban network at mmWave.

## II. SYSTEM MODEL

In this section, we explain the key assumptions and models adopted in this paper. First, we explain street modeling in urban vehicular networks. Then, we introduce a modified mmWave sectorized antenna pattern used for the analysis. We present a tractable form of the pathloss model of mmWave microcells based on Manhattan distance from [27]. Lastly, we formulate the signal-to-noise-plus-interference ratio (SINR) of the receiver and demonstrate the strongest propagation path rule.

### A. Network model : MPLP model

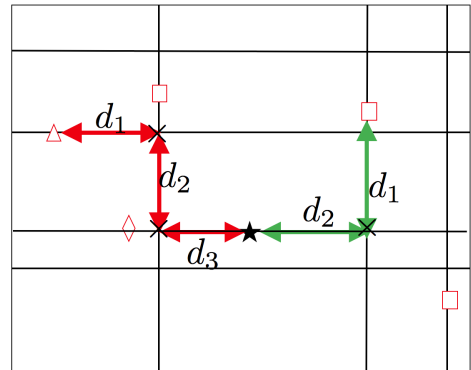


Fig. 1. An illustration of our proposed pathloss model. The  $\star$  is the typical receiver, the diamond  $\diamond$  represents one typical BS,  $\square$  is a cross BS and  $\triangle$  is a parallel BS. The red line denotes the propagation link of a parallel BS and the green line is the propagation path of a cross BS. We use  $\times$  to represent corner loss. The pathloss in decibel scale is added up by the pathloss on each individual segments of the propagation path.

We model the urban area as a stochastic Manhattan type network [15], [33], [34], and the location of the urban streets

<sup>2</sup>Henceforth we assume a downlink so that receiver and UE can be used exchangeably.

are modeled by Manhattan Poisson line process (MPLP). We show in Fig. 1 an illustration of the Manhattan network in the two dimensional Euclidean plane, consisting of the typical street located in the center, cross streets and parallel streets. In particular, we neglect the street width in this paper. Instead of modeling streets with fixed spacings in urban areas, we consider the location of both the cross and parallel streets to be stochastic, which are modeled as homogeneous *Poisson point processes* (PPP). Based on Slivnyak's Theorem, the parallel (including typical) streets and cross street processes are denoted as  $\Psi_S$ , with intensity  $\lambda_S$ . Without loss of generality, we assume the *typical* receiver is located at the origin, on the *typical* street. BSs on the typical/cross and parallel streets are also modeled as independent one-dimensional homogeneous PPPs, and we assume that their intensities are identical, which is  $\lambda_B$ .

### B. Sectorized antenna model

To leverage array gains, directional beamforming by multiple antennas are performed at mmWave BSs. For simplicity, we assume the receiver has an omni-directional antenna, and the BSs are equipped with  $N_t$  transmit antennas. We adopt a sectorized antenna model for the BS as [14], [28], with the main lobe gain denoted as  $G$  and the side-lobe gain as  $g$ . The beamwidth of the main lobe is  $\theta = \frac{2\pi}{\sqrt{N_t}}$  and all the other directions outside the main lobe are assumed to be in the side lobe. The receiver can be aligned with either the main lobe or the side lobe. Since the beamforming direction of the BS is assumed to be uniformly distributed in  $(0, 2\pi)$ , the beamforming antenna gain  $\mathcal{G}$  of one typical BS with LOS visibility to the typical receiver is a Bernoulli random variable, so that

$$\mathcal{G} = \mathbb{I}(p)G + \mathbb{I}(1-p)g, \quad (1)$$

where

$$p = \frac{\theta}{2\pi}. \quad (2)$$

For a uniform planar antenna array, the main lobe gain can be approximated by  $G = N_t$ , which is the maximum power gain that can be supported with  $N_t$ -element antenna array. The side-lobe gain is approximated by  $g = \frac{\sqrt{N_t} - \frac{\sqrt{3}}{2\pi} N_t \sin\left(\frac{\sqrt{3}}{2\sqrt{N_t}}\right)}{\sqrt{N_t} - \frac{\sqrt{3}}{2\pi} \sin\left(\frac{\sqrt{3}}{2\sqrt{N_t}}\right)}$  [28].

### C. Pathloss model

We adopt a pathloss model that is based on the Manhattan distance instead of Euclidean distance. The model is similar to [27], but uses several modifications to provide tractability. Ray tracing shows that in an urban microcell, Euclidean distance might not be a dominant parameter in pathloss modeling. Instead, the street orientation relative to the BS location, and the absolute position of the BS and receiver are the key parameters to determine the pathloss.

It is shown by the ray tracing results that to calculate the pathloss of a propagation link in urban mmWave microcells, the pathloss on different segments of the propagation paths

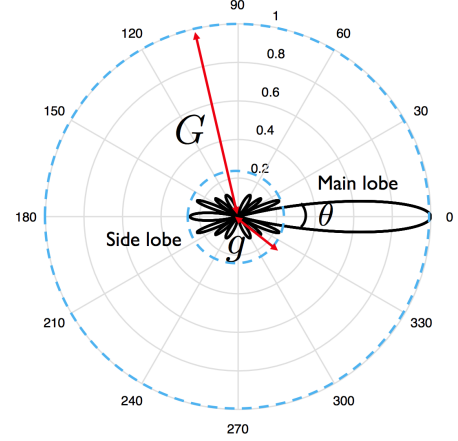


Fig. 2. An illustration of the simplified sectorized antenna pattern. The example is drawn from a uniform planar array (ULA) with transmit antenna number  $N_t = 8$ . We only consider the main lobes and the side lobes. Main lobes and side lobes are assumed to have identical gain on different directions, respectively denoted by  $G$  and  $g$ .

should be added up, with an additional loss when the waves couple into a new street canyon, in urban mmWave microcells. We assume that there are in total  $M$  segments of the propagation paths, i.e.,  $M - 1$  corners along the propagation path where signal change directions. Note that the value of  $M$  depends on the actual position of the BS and the receiver. The individual length of the  $i$ th segment is denoted as  $d_i$ , the pathloss exponent on the  $i$ th segment is  $\alpha_i$ , the corner loss at the corner of the  $i$ th the street segment and  $i + 1$ th segment is  $\Delta$  (in decibel scale), where we assume corner losses at different corners are identical.

We define the *LOS segment* as the first segment of the propagation path from the BS and *NLOS segment* as the remaining segments on the propagation path. We assume that LOS segments on different streets share the same pathloss exponent  $\alpha_L$ , while the pathloss exponent for NLOS segments is  $\alpha_N$ . Considering the sectorized antenna model at the BS, we incorporate the beamforming gain in the definition of the pathloss, and formulate the pathloss in decibel scale as

$$\text{PL}_{\text{dB}} = 10 \left( \alpha_L \log_{10} d_1 + \alpha_N \sum_{i=2}^M \log_{10} d_i \right) + (M - 1)\Delta - \mathcal{G}_{\text{dB}}, \quad (3)$$

where the last term  $\mathcal{G}_{\text{dB}}$  is the random beamforming gain of the sectorized antenna model from (1) in decibel scale. With this Manhattan distance based pathloss model, we can classify the BSs into three categories, as illustrated in Fig. 1: i) BSs on the typical street (typical BSs) that have one direct propagation path to the typical receiver; ii) NLOS BSs on the cross streets (cross BSs) that have a propagation path consisting of a LOS segment (green path  $d_1$ ) and NLOS segment (green path  $d_2$ ) to the typical receiver, and iii) NLOS BSs on the parallel streets (parallel BSs) that have a propagation path consisting of a LOS segment (red path  $d_1$ ) and two NLOS segments (red path  $d_2, d_3$ ). This pathloss model also bears a strong relationship to [35], which considered the pathloss model in urban microcells

where waves are coupled at the street corners with different angles.

#### D. Signal-to-interference-plus-noise ratio (SINR)

SINR coverage analysis is important to determine outage holes and ergodic throughput of the system. While these metrics in the context of mmWave-based vehicular networks depend on both mobility and the blockage effects due to the vehicles, we consider snapshots of the urban microcellular network and look at the distribution of the instantaneous SINR. This approach is taken primarily to confirm the analytic tractability of the pathloss model described in Section II-C, which captures the blockage and shadowing effects due to buildings and accounts for the geometry of streets in an urban environment.

Based on the pathloss model in Section II-C, there are three types of BSs to analyze: typical/cross/parallel BSs. To formulate the SINR, we first make the following assumption of the BS association rule.

**Assumption 1.** *The receiver is associated to the BS with the smallest pathloss, as defined in (3).*

We use  $\Phi_T$  to denote the set of LOS link distances  $x_T$  from the typical BSs to the receiver. The set of lengths of the horizontal and vertical links,  $x_C$  ( $d_1$  in green) and  $y_C$  ( $d_2$  in green), constituting the propagation path from the cross BSs is denoted as  $\Phi_C$ . Similarly,  $\Phi_P$  is used to denote the set of distances  $(x_P, y_P, z_P)$  ( $d_3, d_2, d_1$  in red) corresponding to the propagation path from parallel BSs (see Fig. 1). To simplify demonstration, we define the path gain of the LOS and NLOS segment respectively as  $\ell_L(x)$  and  $\ell_N(x)$ .

$$\ell_L(x) = \mathcal{G}x^{-\alpha_L}, \quad (4)$$

and

$$\ell_N(x) = cx^{-\alpha_N}, \quad (5)$$

where  $x$  is the length of the propagation segment,  $\mathcal{G}$  is the random beamforming gain for each BS defined in (1). It should be noted that the beamforming gain is added only to the LOS segment pathloss. This is based on the definition that the LOS segment is the first path from the BS, hence with beamforming gain included; the corner loss term  $c = 10^{-\Delta/10}$  in the total path gain expression is also captured along with the propagation loss in the NLOS segment in (5), with  $\alpha_N$  denoting the NLOS pathloss exponent.

Conditioning on the associated link gain as  $u$ , the SINR can be formulated as follows, in terms of interference components, respectively from the typical BSs  $I_{\phi_T}$ , cross BSs  $I_{\phi_C}$  and parallel BSs  $I_{\phi_P}$ ,

$$\text{SINR} = \frac{h_o u}{N_0 + I_{\phi_T}(o) + I_{\phi_C}(o) + I_{\phi_P}(o)}, \quad (6)$$

$$\text{with } I_{\phi_T}(o) = \sum_{x_T^i \in \Phi'_T} h_i \ell_L(x_T^i), \quad (7)$$

$$I_{\phi_C}(o) = \sum_{(x_C^i, y_C^i) \in \Phi'_C} h_i \ell_N(x_C^i) \ell_L(y_C^i), \quad (8)$$

$$\text{and } I_{\phi_P}(o) = \sum_{(x_P^i, y_P^i, z_P^i) \in \Phi'_P} h_i \ell_N(x_P^i) \ell_N(y_P^i) \ell_L(z_P^i). \quad (9)$$

Based on Assumption 1 and conditioning on the associated link gain as  $u$ , we have the following constraints for the set  $\Phi'_T, \Phi'_C$  and  $\Phi'_P$  in (7) – (9) as

$$\Phi'_T = \{x_T \in \Phi_T \mid \ell_L(x_T) < u\}, \quad (10)$$

$$\Phi'_C = \{(x_C, y_C) \in \Phi_C \mid \ell_N(x_C) \ell_L(y_C) < u\}, \quad (11)$$

$$\text{and } \Phi'_P = \{(x_P, y_P, z_P) \in \Phi_P \mid \ell_N(x_P) \ell_N(y_P) \ell_L(z_P) < u\}. \quad (12)$$

Based on the strongest BS association rule in Assumption 1, all interfering BSs should have smaller path gain than  $u$ , which leads to (7) – (9).

#### E. Strongest propagation path of a parallel BS

Though there could be multiple propagation paths to the typical receiver and the actual received power is the sum of received signal power from different paths, to make the analysis tractable, we have the following assumption.

**Assumption 2.** *There is one unique path from any BS to the typical receiver (for analysis), which provides the largest path gain.*

This assumption retains the key features of channels, by capturing the strongest path of the channel.

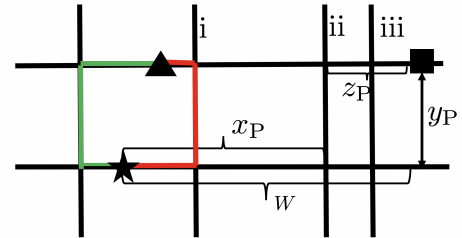


Fig. 3. An illustration of propagation paths from a parallel BS. The star represents the receiver. The rectangle is a BS located in a different block as the receiver while the triangle denotes a BS located in the same block.

To be the strongest path, the path should have i) shorter individual path segment lengths, ii) fewer individual segments, hence fewer corners and smaller corner loss (pathloss is calculated by multiplying individual segment pathloss and one extra multiplication might reduce the pathloss by orders of magnitude), iii) larger beamforming gain. Clearly, the strongest paths from the typical BSs and cross BSs are unique. For typical BSs, the strongest path is just the direct link between the BS and receiver; for cross BSs, the strongest path comprises the vertical link from the BS to the corner of the street the receiver is located on and the horizontal segment from this corner to the receiver, as illustrated by the green paths in Fig. 1. For the parallel BSs, however, the identification of the strongest path is not straightforward. There might be multiple propagation paths that could become the strongest path. Also, the strongest path could come from either main lobes or side lobes, which have different beamforming gains.

First, the strongest path consists of only two corners, which means it has three individual segments (two NLOS and one LOS). We first provide Fig. 3 to demonstrate the problem. For a parallel BS located in the same block as the receiver (example marked by the triangle in Fig. 3), it is clear that the strongest path is either the *left* path (outlined in green) or the *right* path (outlined in red). For parallel BSs in different blocks as the receiver (see rectangle in Fig. 3). We denote the distance from the receiver to the cross street as  $x_P$ , the distance from the BS to the cross street as  $z_P$ . The distance between the parallel street of the BS and the typical street as  $y_P$ , and the horizontal distance between the receiver and the BS is  $W = x_P + z_P$ .

It should be noted that the largest path gain could be via any of the cross streets between the receiver and the transmitter or via a cross street closest to the transmitter, that does not lie in between the receiver and the transmitter. We make the following assumption.

**Assumption 3.** *For the strongest path of the parallel BSs, the signal travels along the LOS segment (first segment of the path) in the direction towards the receiver, rather than away from it.*

With this assumption, for a parallel BS (example marked by *rectangle* in Fig. 3) located in the different block as the receiver, the strongest path can be via any of the cross street as i, ii, iii (lying between receiver and BS), as shown in Fig. 3. To find the strongest path for the parallel BS at different blocks as the receiver, we provide the following proposition.

**Proposition 1.** *The strongest propagation path from a parallel BS is via either the cross street  $\Theta_R$  closest to the receiver or  $\Theta_B$  closest to the BS.*

*Proof.* Conditioning on the location of the parallel BS, the segment  $y_P$  and the corner loss  $2\Delta$  of all propagation paths are the same, hence, the pathloss on the vertical link and the two corner losses can be taken out while formulating the following optimization problem.

Since  $\mathcal{G}$  is a random variable taking values of  $G$  or  $g$ , as defined in (1), we have  $\mathcal{G} \leq G$ . Hence, the maximum path gain of the parallel BS  $G_P$  can be upper bounded by

$$\begin{aligned} G_P &\leq G - 2\Delta - 10\alpha_N \log_{10} y_P + 10G_M \\ &\leq G - 2\Delta - 10\alpha_N \log_{10} y_P + 10 \max\{G_M\}. \end{aligned} \quad (13)$$

where

$$G_M = -\alpha_N \log_{10} x_P - \alpha_L \log_{10} z_P. \quad (14)$$

We then formulate the optimization problem of  $G_M$  as

$$\begin{aligned} &\underset{x_P, z_P \in (0, W)}{\text{maximize}} && -\alpha_N \log_{10} x_P - \alpha_L \log_{10} z_P \\ &\text{subject to} && x_P + z_P = W \end{aligned} \quad (15)$$

The objective function can be expressed as  $P(x) = -\alpha_N \log x - \alpha_L \log(W - x)$ ,  $x \in (0, W)$ , whose second order derivative is

$$P''(x) = \frac{\alpha_N}{x^2} + \frac{\alpha_L}{(W - x)^2}, \quad (16)$$

The second order derivative of  $P(x)$  is positive for all  $\alpha_L$ ,  $\alpha_N$ , and  $W$ , which means  $P(x)$  is convex. Denoting the distance from  $\Theta_R$  to the receiver as  $x_1$  and the distance from  $\Theta_B$  to the BS as  $x_2$ , and using the convexity of  $P(x)$ , we have

$$\begin{aligned} P(\lambda x_1 + (1 - \lambda)x_2) &< \lambda P(x_1) + (1 - \lambda)P(x_2) \\ &< \max\{P(x_1), P(x_2)\} \quad \forall \lambda \in (0, 1) \text{ and } x_1, x_2 \in (0, W). \end{aligned} \quad (17)$$

In (17),  $P(\lambda x_1 + (1 - \lambda)x_2)$  parameterizes all path gains of the propagation paths via any cross street lying between  $\Theta_R$  and  $\Theta_B$ . From the second inequality in (17), all these propagation paths have smaller path gain than that going through the streets specified in this proposition, which concludes the proof.  $\square$

Since the pathloss exponent of the segment  $z_P$  is  $\alpha_L$  and that of the segment  $x_P$  is  $\alpha_N$ , with  $\alpha_L < \alpha_N$ , it is intuitive that the strongest path is more likely to be via the street *closest to the receiver*, i.e.,  $\Theta_R$ .

To conclude the discussion on the uniqueness of the propagation path in the system model considered in this paper, we demonstrated that for both the typical and cross BSs, the propagation path is unique and also easy to identify based on the strongest path gain association criterion. For the parallel BS, irrespective of whether the BS is located in the same block as the receiver, there are only two potential paths to be the strongest, and for analysis, we choose the path closest to the receiver.

### III. COVERAGE ANALYSIS

In this section, we compute the coverage probability of a typical receiver in the MPLP microcellular network. First, we explain the independent thinning of the BSs considering the sectorized beam pattern of the mmWave BSs. Then, we analyze the CDF of the associated link path gain based on strongest BS association rule in Assumption 1. In addition, we derive an accurate and concise expression of the coverage probability. Finally, we examine the effects of LOS and NLOS interference in MPLP network.

#### A. Independent thinning of BSs

Based on the sectorized antenna model in Section II-B, the BSs are thinned with probability  $p_T$  and  $1 - p_T$ , respectively, which then generate two independent Poisson point processes of BSs with antenna gain of  $G$  and  $g$  respectively. After the independent thinning, the densities of the independent thinning of BSs with antenna gain of  $G$  and  $g$  are respectively

$$\lambda_b = p_T \lambda_B \quad \text{and} \quad \bar{\lambda}_b = (1 - p_T) \lambda_B. \quad (18)$$

For typical and cross BSs, the thinning probability  $p_T = p$ , which is the probability that the receiver lies inside the main lobe, as defined in (2). We consider the same independent BS thinning rule for typical and cross BSs, even though it is not necessarily applicable for both cases. For example, for a cross BS, if the side lobe is aligned with the street corner with the typical street, the main lobe, which points to the other direction, might still be able to detour its way and reach the receiver. Yet the assumption we make here is

reasonable, since the *detoured* instead of the direct path with the smallest pathloss introduces at least one extra corner loss, which attenuates the signal a lot. This justifies the assumption and validates the independent thinning of both the typical and cross BSs.

For the parallel BSs, however, as has been mentioned in the uniqueness analysis of the strongest path in Section II-C, half of the parallel BSs are pointing to one side with beamforming gain as  $G$ , while the other half are pointing to a different location with gain as  $g$ . Hence, the parallel BSs are thinned with a probability of  $p_T = \frac{1}{2}$  with main lobe and side lobe gain respectively.

### B. Distribution of associated link gain

To simplify SINR coverage analysis, we assume all links experience independent and identically distributed (I.I.D.) Rayleigh fading with mean 1,  $h \sim \exp(1)$ . We denote the normalized transmit power  $P_B = 1$  and represent the noise by  $N_0$ . Since the SINR expression in (6) is conditioned on the associated link gain  $u$ , we first analyze the distribution of  $u$ . Based on the BS association law in Assumption 1, the receiver can be associated to either a typical/cross or parallel BS. The following lemma provides the cumulative density function (CDF) of the largest gain from the typical/cross/parallel BS respectively.

**Lemma 1.** *The CDFs of the largest gain of the typical BSs  $u_1 = \max_{(x_T \in \Phi_T)} \{\ell_L(x_T)\}$ , cross BSs  $u_2 = \max_{(x_C, y_C) \in \Phi_C} \{\ell_N(x_C)\ell_L(y_C)\}$  and parallel BSs  $u_3 = \max_{(x_P, y_P, z_P) \in \Phi_P} \{\ell_N(x_P)\ell_N(y_P)\ell_L(z_P)\}$  are given or bounded by*

$$F_{u_T}(u) = \exp\left(-\gamma_T \lambda_B u^{-\frac{1}{\alpha_L}}\right), \quad (19)$$

$$F_{u_C}(u) = \exp\left(-\gamma_C \lambda_B^{\frac{\alpha_L}{\alpha_T}} u^{-\frac{1}{\alpha_N}}\right), \quad (20)$$

$$F_{u_P}(u) \geq 2\lambda_S \sqrt{\frac{2\gamma_P \lambda_B^{\frac{\alpha_L}{\alpha_N}} u^{-\frac{1}{\alpha_N}}}{\lambda_S}} K_1\left(2\sqrt{2\gamma_P \lambda_S \lambda_B^{\frac{\alpha_L}{\alpha_T}} u^{-\frac{1}{\alpha_N}}}\right), \quad (21)$$

where

$$\gamma_T = 2p_T G^{\frac{1}{\alpha_L}} + 2(1 - p_T)g^{\frac{1}{\alpha_L}}, \quad (22)$$

$$\gamma_C = \gamma_{C1}\gamma_{C2}, \quad (23)$$

$$\gamma_{C1} = 2^{\frac{\alpha_L}{\alpha_N} + 1} \lambda_S c^{\frac{1}{\alpha_N}} \Gamma\left(1 - \frac{\alpha_L}{\alpha_N}\right), \quad (24)$$

$$\gamma_{C2} = \left(p_T^{\frac{\alpha_L}{\alpha_N}} G^{\frac{1}{\alpha_N}} + (1 - p_T)^{\frac{\alpha_L}{\alpha_N}} g^{\frac{1}{\alpha_N}}\right), \quad (25)$$

$$\gamma_P = \gamma_{C1} c^{\frac{1}{\alpha_N}} G^{\frac{1}{\alpha_N}}, \quad (26)$$

and  $K_1(\cdot)$  is the 1-st order modified Bessel's function of the second kind [36].

*Proof.* See Appendix A.  $\square$

Based on properties of the modified Bessel function, when the argument  $\mu$  of  $K_1(\mu)$  becomes small, we can approximate

it as [37]

$$K_1(\mu) \sim \mu^{-1}. \quad (27)$$

The argument  $\gamma_P \lambda_B^{\frac{\alpha_L}{\alpha_N}}$  inside the modified Bessel function in (19)  $\gamma_P \ll 1$ , since it scales with  $\lambda_S \lambda_T^{\frac{\alpha_L}{\alpha_N}}$  which is generally very small. The corner loss term further reduces the value to a large extent, so that (27) applies. Consequently, we can approximate (19) as

$$\begin{aligned} F_{u_P}(u) &\approx 2\lambda_S \sqrt{\frac{2\gamma_P \lambda_B^{\frac{\alpha_L}{\alpha_N}} u^{-\frac{1}{\alpha_N}}}{\lambda_S}} \left(2\sqrt{2\gamma_P \lambda_S \lambda_B^{\frac{\alpha_L}{\alpha_N}} u^{-\frac{1}{\alpha_N}}}\right)^{-1} \\ &= 1, \end{aligned} \quad (28)$$

which implies that generally the largest gain from a parallel BS is very small, that is, the probability of associating with a parallel BS is negligible.

Using Lemma 1, the distribution of the associated link path gain  $U = \max\{u_T, u_C, u_P\}$  can be evaluated as

$$\begin{aligned} F_U(u) &= \mathbb{P}(\max\{u_T, u_C, u_P\} < u) \\ &\stackrel{(a)}{=} \mathbb{P}(u_T < u, u_C < u, u_P < u) \\ &\stackrel{(b)}{\approx} \exp\left(-\gamma_T \lambda_B u^{-\frac{1}{\alpha_L}}\right) \exp\left(-\gamma_C \lambda_B^{\frac{\alpha_L}{\alpha_N}} u^{-\frac{1}{\alpha_N}}\right), \end{aligned} \quad (29)$$

where (a) is based on the fact that the locations of the typical/cross/parallel BSs are mutually independent, (b) follows the results of Lemma 1 that the association with parallel BSs is negligible. Fig. 4 compares the numerically evaluated CDF of the associated link gain of association only with typical BSs, with typical/cross BSs and considering all association cases, against the theoretical result given in (29). It is seen that the analytic result matches well with the numerical result. It can also be seen that the empirical CDF curves obtained with and without the association with the parallel BSs coincide. This verifies the analysis in Lemma 1 and the subsequent approximation for largest gain seen by parallel BSs. Also, the curve shows that the cross BSs association is very small compared to the typical BSs association.

### C. Coverage probability

In this section, we derive a closed-form expression for the coverage probability  $p_c(u, T)$  conditioned on the associated link gain as  $u$ . The coverage probability conditioned on  $u$  is defined as

$$p_c(u, T) = \mathbb{P}(\text{SINR} > T | u). \quad (30)$$

Using (6) – (9), (30) can be expanded in terms of the Laplace transforms of interference and noise as follows.

$$\begin{aligned} p_c(u, T) &= \mathbb{P}(h > Tu^{-1}(N_0 + I_{\phi_T}(o) + I_{\phi_V}(o) + I_{\phi_H}(o))) \\ &\stackrel{(a)}{=} \exp(-Tu^{-1}N_0) \mathcal{L}_{I_{\phi_T}}(Tu^{-1}) \mathcal{L}_{I_{\phi_C} + I_{\phi_P}}(Tu^{-1}), \end{aligned} \quad (31)$$

where (a) is based on the assumption of i.i.d. Rayleigh fading channels, and  $\mathcal{L}(\cdot)$  is the Laplace transform (LT) of random variable  $(\cdot)$ . Note that we cannot completely decouple the interference terms since the propagation links from the cross



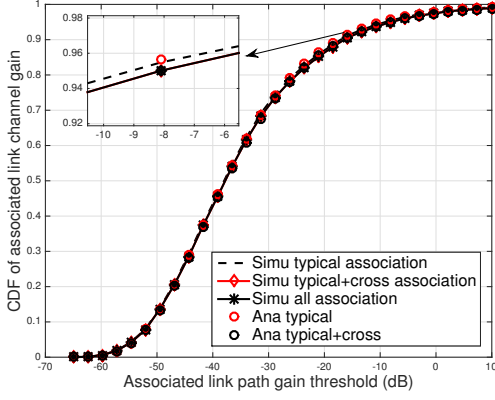


Fig. 4. Comparison of analytic and numerical associated link gain distribution. The black dashed line represents the association with only the typical BSs, the red solid line is the CDF considering association with both typical and cross BSs, and the black solid line is the result of considering all association cases. The red circle and black circle respectively denote the analytic result of CDF of associated gain with only typical BS association and typical/cross BS association.

and parallel BSs share the same path segments thus making their individual interference not independent. To analyze the problem, we start with examining the parallel BS interference.

**Proposition 2.** A lower bound of LT of the interference from the parallel BSs  $I_{\phi_P}$  is

$$\mathcal{L}_{I_{\phi_P}}(Tu^{-1}) \geq 2\lambda_S \sqrt{\frac{2\gamma_P (\lambda_B \varrho(T))^{\frac{\alpha_L}{\alpha_N}} u^{-\frac{1}{\alpha_N}}}{\lambda_S}} \times K_1 \left( 2\sqrt{2\gamma_P \lambda_S (\lambda_B \varrho(T))^{\frac{\alpha_L}{\alpha_N}} u^{-\frac{1}{\alpha_N}}} \right) \approx 1, \quad (32)$$

where  $\gamma_P$  is defined in (22), and

$$\varrho(T) = \int_1^\infty \frac{1}{1 + T^{-1}\mu^{\alpha_L}} d\mu. \quad (33)$$

*Proof.* The proof follows from the proof of Lemma 1 given in Appendix A.  $\square$

Since the LT of the parallel interference evaluates to 1 approximately, which indicates that the interference from parallel BSs is small enough to be neglected, i.e.,  $I_{\phi_P} \approx 0$ . Hence, the coverage probability in (34) can be reformulated as

$$p_c(u, T) = \exp(-Tu^{-1}N_0) \mathcal{L}_{I_{\phi_T}}(Tu^{-1}) \mathcal{L}_{I_{\phi_C}}(Tu^{-1}), \quad (34)$$

which is derived in the following Theorem.

**Theorem 1.** The coverage probability conditioned on the channel gain  $u$  of the associated link is

$$p_c(u, T) = \exp(-\beta_1 u^{-1}) \exp(-\beta_2 \lambda_B u^{-\frac{1}{\alpha_L}}) \times \exp\left(-\beta_3 \lambda_B^{\frac{\alpha_L}{\alpha_N}} u^{-\frac{1}{\alpha_N}}\right), \quad (35)$$

where

$$\begin{aligned} \beta_1 &= TN_0, & \beta_2 &= \gamma_T \varrho(T), \\ \beta_3 &= \gamma_C \varrho(T)^{\frac{\alpha_L}{\alpha_N}}, \end{aligned} \quad (36)$$

and  $\varrho(T)$  is defined in (33).

*Proof.* See Appendix B.  $\square$

Using Theorem 1 and the distribution of the associated link path gain in (29), the SINR coverage probability can be evaluated as

$$P_c(T) = \int_0^\infty p_c(u, T) f_U(u) du, \quad (37)$$

where  $p_c(u, T)$  is provided in (35), and the probability density function (PDF)  $f_U(u)$  can be obtained from the CDF derived in (29).

Though the coverage probability serves as an important metric in evaluating performance, it is not sufficient to characterize how much data rate the system can support. We next use a simplified definition of throughput  $\mathcal{T}(\beta)$  to quantify the data rate,

$$\mathcal{T}(\eta) = \log_2(1 + \eta) P_c(\eta), \quad (38)$$

where  $\eta$  is the SINR threshold and  $P_c(\eta)$  is the coverage probability given in (37).

#### D. The effect of LOS and NLOS interferers

In Proposition 2, we showed that the parallel BSs interference can be neglected in the analysis. In this section, we further compare the effects of typical interference  $\phi_T$  and cross interference  $\phi_C$ . For tractable analysis, we assume the receiver is associated to the typical BS, so that we can have simpler associated link gain distribution. The analysis is based on the application of Jensen's inequality to the individual LT of  $I_{\phi_T}$  and  $I_{\phi_C}$ .

From Theorem 1, the LT of the interference of BSs on the typical street is  $\mathcal{L}_{I_{\phi_T}}(T, u) = \mathbb{E}_u \left[ \exp \left( -\beta_2 \lambda_B u^{-\frac{1}{\alpha_L}} \right) \right]$  and the LT of the interference due to the NLOS BSs on the cross streets is  $\mathcal{L}_{I_{\phi_C}}(T, u) = \mathbb{E}_u \left[ \exp \left( -\beta_3 \left( \lambda_B u^{-\frac{1}{\alpha_L}} \right)^{\frac{\alpha_L}{\alpha_N}} \right) \right]$ . Define two convex functions  $\varphi_1(u) = \exp(-u)$  and  $\varphi_2(u) = \exp(-u^{\frac{\alpha_L}{\alpha_N}})$ . Since we assume the BS is associated to one typical BS in this case, the CDF of the associated link path gain  $u$  becomes

$$F(u) = \exp \left( -\gamma_T \lambda_B u^{-\frac{1}{\alpha_L}} \right). \quad (39)$$

By change of variables, we can obtain

$$\mathbb{E}_u \left[ u^{-\frac{1}{\alpha_L}} \right] = \frac{1}{\gamma_T \lambda_B}, \quad (40)$$

hence, by Jensen's inequality, the lower bound of  $\mathcal{L}_{I_{\phi_T}}(T, u)$  becomes

$$\mathcal{L}_{I_{\phi_T}}(T, u) \geq \mathcal{L}_{I_{\phi_T}}^{\text{LB}}(T, u) = \exp \left( -\frac{\beta_2}{\gamma_T} \right) = \exp(-\varrho(T)). \quad (41)$$

Similarly, we have

$$\mathbb{E}_u \left[ \left( \lambda_B u^{-\frac{1}{\alpha_L}} \right)^{\frac{\alpha_L}{\alpha_N}} \right] = \left( \frac{1}{\gamma_T} \right)^{\frac{\alpha_L}{\alpha_N}} \Gamma \left( 1 + \frac{\alpha_L}{\alpha_N} \right), \quad (42)$$

with the lower bound of  $\mathcal{L}_{I_{\phi_C}}(T, u)$  evaluated as

$$\mathcal{L}_{I_{\phi_C}}^{\text{LB}}(T, u) = \exp \left( - \left( \frac{1}{\gamma_T} \right)^{\frac{\alpha_L}{\alpha_N}} \beta_3 \Gamma \left( 1 + \frac{\alpha_L}{\alpha_N} \right) \right) = \exp \left( - \frac{2^{\frac{\alpha_L}{\alpha_N} + 1} \lambda_S c^{\frac{1}{\alpha_N}} \Gamma \left( 1 - \frac{\alpha_L}{\alpha_N} \right) \Gamma \left( 1 + \frac{\alpha_L}{\alpha_N} \right) \gamma_{C2}}{\gamma_T^{\frac{\alpha_L}{\alpha_N}}} \varrho(T)^{\frac{\alpha_L}{\alpha_N}} \right). \quad (43)$$

Note that the argument inside (43) scales with  $\lambda_S$  and  $c^{\frac{1}{\alpha_N}}$ , which makes the inside argument very small, therefore, it holds

$$\mathcal{L}_{I_{\phi_C}}^{\text{LB}}(T, u) \ll \mathcal{L}_{I_{\phi_C}}^{\text{LB}}(T, u) \approx 1. \quad (44)$$

From (43), it can be seen that the lower bound of LT of  $I_{\phi_C}$  scales exponentially with  $\beta_3 = \gamma_C \varrho(T)^{\frac{\alpha_L}{\alpha_N}}$ , which further scales with  $\lambda_S c^{\frac{1}{\alpha_N}}$ . This leads to an intuitive insight that when the street intensity increases, the effects by cross BS interference grow larger. It should be noted from (44), that the cross BS interference is very small compared to typical BSs. And generally, the cross interference can be neglected, with a relatively large corner loss  $\Delta$ .

Fig. 5 gives a comparison between the analytic and simulation results of the coverage probability when considering no interference (noise only), considering interference from only typical BSs, and both typical and cross BS interference, and all of the interference. It is shown that the coverage probabilities with and without the parallel BSs completely coincide. This verifies the corresponding proof in Proposition 2 that the parallel interference can be neglected. It can also be observed that the cross BS interference is also negligible compared to the typical BS interference, which is demonstrated in the Jensen's inequality lower bound analysis in (41) and (43). We set the corner loss in the simulation as  $\Delta = 20\text{dB}$ , and in this setting, we can conclude that under the Manhattan distance based pathloss model, the NLOS interference (from cross/parallel BSs) is negligible. It will also be shown in Section IV that with the corner loss ranging from 30dB to 0dB (no shadowing loss case), the coverage probability does not vary significantly. This indicates that whatever the corner loss is, the NLOS interference is always very small compared to the LOS interference.

#### IV. SCALING LAW OF COVERAGE PROBABILITY WITH NETWORK INTENSITIES

The coverage probability serves as an important metric in evaluating system performance, since it is closely related to ergodic rate and throughput outage. In this section, we focus on answering the following questions: i) how densely should BSs be deployed in urban streets to maximize coverage at a minimum cost? ii) how does the coverage probability change for different densities in different cities?

##### A. Scaling law with BS intensity

The interference limited scenario targets an asymptotic case, where the noise can be neglected and thus focus fully on the interplay between network intensities. This scenario can

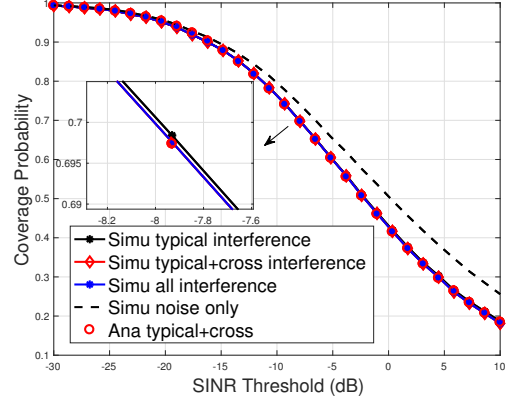


Fig. 5. Comparison of the numerical and analytic coverage probability. The black/red/blue solid lines respectively represent the coverage probability considering only typical BS interference, both typical and cross BS interference and all interference. The black dashed line is the coverage probability simulated considering noise only. Red circles are the analytic expression of coverage probability in (35) – (37) considering interference from typical and cross BSs.

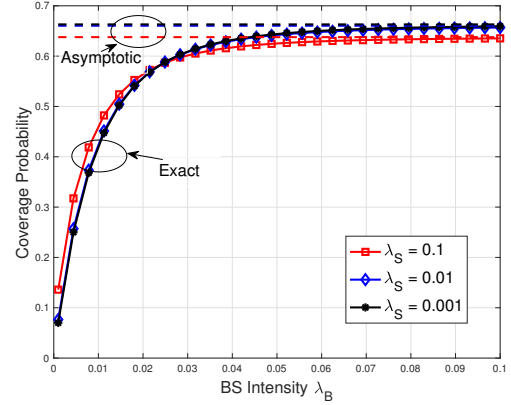


Fig. 6. Asymptotic behavior of coverage probability with large BS intensity  $\lambda_B$ . Solid red, green and blue curves are respectively the coverage probability under different street intensities,  $\lambda_S = 0.1, 0.01$  and  $0.001$ . Dashed curves represent the analytic asymptotic value of the coverage probability when BS intensity grows very large.

either be achieved by very high BS intensity or by very dense streets deployment. Based on the coverage probability given in (35) and (36), after neglecting the noise term and changing variables by  $x = \lambda_B u^{-\frac{1}{\alpha_L}}$ , the expression of the coverage probability becomes

$$P_c(T) = \int_0^\infty \exp(-(\beta_2 + \gamma_T)x) \exp\left(-(\beta_3 + \gamma_C)x^{\frac{\alpha_L}{\alpha_N}}\right) \times \left(\gamma_T + \frac{\gamma_C \alpha_L}{\alpha_N} x^{\frac{\alpha_L}{\alpha_N} - 1}\right) dx, \quad (45)$$

where  $\beta_2$ ,  $\beta_3$ ,  $\gamma_T$  and  $\gamma_C$  are provided in Section III.

Under the modeling of BSs as PPPs and the Manhattan distance pathloss model, one interesting observation from (45) is that the coverage probability is independent of the BS intensity. On one hand, when both street and BSs intensities grow very large, it is intuitive that with ultra dense deployment of BSs, i.e.,  $\lambda_B \rightarrow \infty$ , both the associated path gain and inter-



ference become very large, and their effects on the coverage probability cancel out, which leads to an asymptotic value of the coverage probability. On the other hand, when only the street intensity itself grows very large, the scenario could also be interference limited. In this case, the coverage probability is still a constant, however densely the BSs are deployed. This reveals an important insight that when street intensity grows large, the increase of coverage probability by deploying denser BSs is less significant. We plot Fig. 6 to demonstrate the above two observations in an ultra-dense network where intensity of BS grows very large. First, it is shown that from approximately  $\lambda_B = 0.05$  (BS spacing of 20m) for different street intensities, the coverage probability starts to converge to the asymptotic value. Second, with denser street distribution (e.g.,  $\lambda_S = 0.1$ , red curve), the increase of coverage probability is less prominent. Also, denser street distribution leads to lower asymptotic coverage probability.

### B. Scaling law with street intensity

In the last section, we demonstrated the impact of different city streets (with different intensities) on the coverage probability enhancement. Next, we reveal the relationship between the coverage probability and the urban street intensity. One important thing to note is that in the dense street case, the street intensity  $\lambda_S$  is not arbitrarily large, where the most dense street might be at least 20m spacing, with  $\lambda_S = 0.05$ . We provide the following proposition to quantify how the coverage probability changes under different street intensities and prove it herein.

**Proposition 3.** 1) When the BS intensity  $\lambda_B$  is large, the coverage probability decreases linearly with the street intensity  $\lambda_S$ . 2) When  $\lambda_B$  is small, the coverage probability increases linearly with  $\lambda_S$ .

*Proof.* In terms of the linear scaling law and its dependence on the BS intensity, we provide the following steps of the proof:

#### 1) Linear scaling law

First, from (35) – (37), the coverage probability can be rewritten as

$$P_c(T) = P_1 + P_2, \quad (46)$$

where

$$P_1 = \int_0^\infty \exp(-\beta_1 u^{-1}) \exp\left(-(\beta_2 + \gamma_T)\lambda_B u^{-\frac{1}{\alpha_L}}\right) \times \exp\left(-(\beta_3 + \gamma_C)\lambda_B^{\frac{\alpha_L}{\alpha_N}} u^{-\frac{1}{\alpha_N}}\right) \left(\frac{\lambda_B \gamma_T}{\alpha_L} u^{-\frac{1}{\alpha_L}-1}\right) du, \quad (47)$$

and

$$P_2 = \int_0^\infty \exp(-\beta_1 u^{-1}) \exp\left(-(\beta_2 + \gamma_T)\lambda_B u^{-\frac{1}{\alpha_L}}\right) \times \exp\left(-(\beta_3 + \gamma_C)\lambda_B^{\frac{\alpha_L}{\alpha_N}} u^{-\frac{1}{\alpha_N}}\right) \left(\frac{\gamma_C}{\alpha_N} \lambda_B^{\frac{\alpha_L}{\alpha_N}} u^{-\frac{1}{\alpha_N}-1}\right) du. \quad (48)$$

We then rewrite the second part in (48), by integration by parts, as

$$P_2 = \frac{\gamma_C}{\gamma_C + \beta_3} \int_0^\infty \exp(-\beta_1 u^{-1}) \exp\left(-(\beta_2 + \gamma_T)\lambda_B u^{-\frac{1}{\alpha_L}}\right) \times \frac{\partial \left[ \exp\left(-(\beta_3 + \gamma_C)\lambda_B^{\frac{\alpha_L}{\alpha_N}} u^{-\frac{1}{\alpha_N}}\right) \right]}{\partial u} du \\ = \frac{\gamma_C}{\gamma_C + \beta_3} - \frac{\gamma_C}{\gamma_C + \beta_3} \int_0^\infty \exp\left(-(\beta_3 + \gamma_C)\lambda_B^{\frac{\alpha_L}{\alpha_N}} u^{-\frac{1}{\alpha_N}}\right) \times \frac{\partial \left[ \exp(-\beta_1 u^{-1}) \exp\left(-(\beta_2 + \gamma_1)\lambda_B u^{-\frac{1}{\alpha_L}}\right) \right]}{\partial u} du. \quad (49)$$

In both (49) and (47), only  $\beta_3 = \zeta_1 \lambda_S$ , and  $\gamma_C = \zeta_2 \lambda_S$  depend on  $\lambda_S$ . Further,  $\beta_3$  scales linearly with  $\gamma_C$ , which itself is very small due to the terms  $\lambda_S$  and  $c^{\frac{1}{\alpha_N}}$ . Then, by applying a first-order Taylor approximation  $\exp(-x) \approx 1 - x$  to  $\exp\left(-(\beta_3 + \gamma_C)\lambda_B^{\frac{\alpha_L}{\alpha_N}} u^{-\frac{1}{\alpha_N}}\right) \approx 1 - \lambda_S(\zeta_1 + \zeta_2)\lambda_B^{\frac{\alpha_L}{\alpha_N}} u^{-\frac{1}{\alpha_N}}$  in (47) and (49), we can see  $P_1$  and  $P_2$  scale linearly with  $\lambda_S$ , hence proving the linear scaling law of coverage probability with  $\lambda_S$ . Fig. 7 compares the exact coverage probability in (46) and that with Taylor approximation. It is shown that under different street intensities  $\lambda_S = 0.001, 0.01, 0.02$ , the exact results match well with the Taylor approximations. This verifies the accuracy of using Taylor approximation to prove the linear scaling law. Another observation here is when the street density is relatively small, e.g.,  $\lambda_S = 0.001$ , the coverage probability is insensitive to the NLOS pathloss exponent  $\alpha_N$ , since the coverage almost remains a constant with  $\alpha_N$  ranging from 3 to 10. When streets become dense, the coverage probability decreases faster with growing  $\alpha_N$ . This is consistent with the fact that  $\alpha_N$  only affects pathloss of the NLOS links.

#### 2) Dependence on BS intensity

To demonstrate the different scaling laws of coverage probability with BS intensities, we take out the components in (45), which are dependent on  $\lambda_S$  of the integral, and define it as  $\Upsilon(\lambda_S)$ , which is

$$\Upsilon(\lambda_S) = \exp\left(-\lambda_S(\zeta_1 + \zeta_2)\lambda_B^{\frac{\alpha_L}{\alpha_N}} u^{-\frac{1}{\alpha_N}}\right) \times \left( \frac{\lambda_B \gamma_T}{\alpha_L} u^{-\frac{1}{\alpha_L}-1} + \frac{\lambda_S \zeta_2 \lambda_B^{\frac{\alpha_L}{\alpha_N}}}{\alpha_N} u^{-\frac{1}{\alpha_N}-1} \right), \quad (50)$$

the derivative of which is

$$\Upsilon'(\lambda_S) = \frac{\lambda_B^{\frac{\alpha_L}{\alpha_N}}}{\alpha_N} u^{-\frac{1}{\alpha_N}-1} \exp\left(-\lambda_S(\zeta_1 + \zeta_2)\lambda_B^{\frac{\alpha_L}{\alpha_N}} u^{-\frac{1}{\alpha_N}}\right) \times \left( \zeta_2 - (\zeta_1 + \zeta_2)\alpha_N \left[ \frac{\gamma_T \lambda_B}{\alpha_L} u^{-\frac{1}{\alpha_L}} + \frac{\lambda_S \zeta_2 \lambda_B^{\frac{\alpha_L}{\alpha_N}}}{\alpha_N} u^{-\frac{1}{\alpha_N}} \right] \right). \quad (51)$$

Since the exponential part from (51) is always positive, and  $\zeta_2$  and  $\zeta_1$  are independent of  $\lambda_B$ , it is clear that when  $\lambda_B$  grows large,  $\Upsilon'(\lambda_S) < 0$ , which indicates when intensity of BSs grows large, coverage probability decreases with  $\lambda_S$ .  $\square$

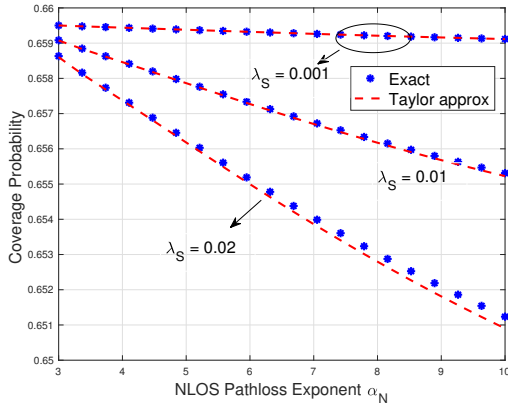


Fig. 7. Comparison of the exact and Taylor approximation of coverage probability. Solid blue curves plot exact coverage probability in Theorem 1 under different street intensities, i.e.,  $\lambda_S = 0.02, 0.01$  and  $0.001$ . The blue stars are the exact coverage probability and the red dashed curves are the Taylor approximations to (47) and (49).

Fig. 8 illustrates the linear scaling of the coverage probability with the intensity of streets  $\lambda_S$ . It first can be observed that the coverage probability scales linearly with the intensity of streets, and the coverage probability increases with  $\lambda_S$  while decreases with corner loss  $\Delta$ , when the BS intensity is relatively small  $\lambda_B = 0.01$ . Also, the coverage probability decreases with  $\lambda_S$  with large BS intensity  $\lambda_B = 0.1$ , while it increases with corner loss in the meantime. This implies that when the BS deployment is dense, interference becomes dominant and larger corner loss reduces the interference; when BSs are relatively sparse, small corner loss strengthens the signal from the cross BSs, thus making the associated link received power stronger and enhancing the coverage probability. Also, it can be observed that when the corner loss becomes small (e.g., the no shadowing loss case  $\Delta = 0$ dB), the coverage probability becomes more sensitive to the change of street intensities, which is shown by a larger slope of the curve of coverage probability. This is because the smaller corner loss makes the cross BS interference more prominent, thus increasing the sensitivity of coverage probability to the street intensities.

It is clear from Section IV-B that the microcellular network does not work efficiently in a scenario where both BS and street intensities are very large. When the BSs are very sparse on each street, increased street intensity makes it more likely to be associated with a BS on cross streets, thus leading to a larger associated path gain. When  $\lambda_B$  grows large, however, the system becomes interference-limited, thus denser streets only contribute to more interference and lower the coverage probability. This sheds light on how to deploy BSs more efficiently under different street intensities. Specifically, when the streets are very dense, relatively sparse BSs should be deployed since coverage probability increases more slowly with more BSs; when the streets are sparse, we could deploy denser BSs to enhance coverage probability (however, too many BSs are inefficient due to the asymptotic behavior of coverage in ultra-dense network).

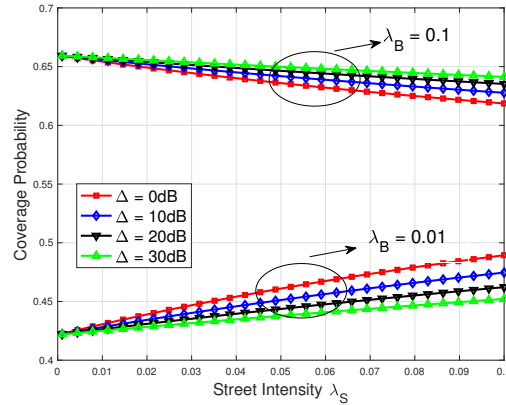


Fig. 8. Scaling of coverage probability with different street intensity  $\lambda_S$ . Comparison is made between sparse/dense BS intensities  $\lambda_B = 0.01, 0.1$  and different corner losses  $\Delta = 0, 10, 20, 30$ dB.

## V. LOS LINK & BS ASSOCIATION ANALYSIS

In this section, we further compute the probability that the link is LOS and analyze the BS association in the MPLP urban microcellular networks. The LOS probability analysis is based on Euclidean distance. The reason for Euclidean distance instead of Manhattan distance based analysis is that we first need the Euclidean distance based LOS probability to calculate the coverage probability and ergodic rate of [14] for pathloss comparison. Also, the MPLP model can be compared to 3GPP urban microcellular comparably since LOS probability in 3GPP is also based on Euclidean distance.

### A. LOS probability

In this section, we analyze the probability the link is LOS under the MPLP model. This result will also be applied to the calculation of pathloss in [14] in Section VI-A for comparison of the new Manhattan distance based model and previous Euclidean distance based pathloss models. We compare the result of the closed-form LOS probability to that in 3GPP microcellular LOS model, which shows a good match between the MPLP LOS probability and the realistic microcellular scenario in 3GPP. This justifies the accuracy of MPLP in urban street modeling.

**Lemma 2.** *In the MPLP, the LOS probability of a propagation link from a BS at Euclidean distance  $d$  is*

$$p_{\text{LOS}}^{\text{MPLP}}(d) = \frac{1 - \exp(-4d\lambda_S)}{4d\lambda_S}. \quad (52)$$

*Proof.* We illustrate the LOS probability analysis in Fig. 9.

According to Slivnyak's theorem [33], [38], [34], we first add a horizontal street  $S_o$  crossing the receiver at  $o$ . Conditioning on the distance between the BS and the receiver as  $d$ , there are in total of  $N_h + 2$  *potential* locations of BSs on the horizontal street and a total number of  $N_v$  *potential* BSs on the cross streets, at an Euclidean distance of  $d$  (which are the intersections of the streets with the circle centered at the receiver  $O$  of radius  $d$ ). Because the streets are modeled

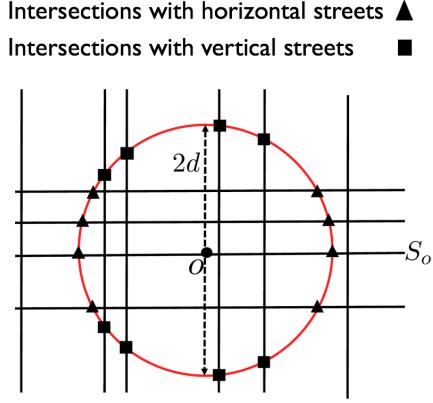


Fig. 9. An illustration of the calculation of LOS probability conditioned on Euclidean distance of the link  $d$ . The red circle has the radius of  $d$ . Rectangles denote the potential locations of BSs with distance  $d$  on the cross streets; Triangles are the potential locations of BSs on the horizontal streets.

as a Poisson line process in the MPLP model,  $N_h$  and  $N_v$  are Poisson random variables with  $\frac{N_h}{2} \sim \text{Poisson}(2\lambda_S d)$  and  $\frac{N_v}{2} \sim \text{Poisson}(2\lambda_S d)$ . Hence, the probability of LOS link is

$$p_{\text{LOS}}^{\text{MPLP}}(d) = \mathbb{E} \left[ \frac{2}{2 + N_h + N_v} \right], \quad (53)$$

which simplifies to

$$\begin{aligned} p_{\text{LOS}}^{\text{MPLP}}(d) &\stackrel{(a)}{=} \sum_{k=0}^{\infty} \frac{(4\lambda_S d)^k}{(1+k)k!} \exp(-4\lambda_S d) \\ &= \frac{\exp(-4\lambda_S)}{4\lambda_S d} \sum_{k=1}^{\infty} \frac{(4\lambda_S d)^k}{k!} \\ &\stackrel{(b)}{=} \frac{1 - \exp(-4d\lambda_S)}{4d\lambda_S}, \end{aligned} \quad (54)$$

where (a) is derived based upon the distribution of Poisson process and (b) utilizes the power series of the exponential function:  $\exp(x) = \sum_{k=0}^{\infty} \frac{x^k}{k!}$ .  $\square$

The LOS probability given in the 3GPP microcellular model is [39]

$$p_{\text{LOS}}^{\text{3GPP}}(d) = \min \left\{ 1, \frac{18}{x} \right\} \left( 1 - \exp \left( -\frac{x}{36} \right) \right) + e^{-\frac{x}{36}}. \quad (55)$$

First, it should be noted that the expression of LOS blockage probability under MPLP model has a similar form as that in the 3GPP microcellular model. By fitting the result to 3GPP microcellular LOS probability in (55) with a minimum mean squared error regression, the street intensity is  $\lambda_S = 0.0092$  (we use  $\lambda_S = 0.01$  in simulations). The comparison in Fig. 10 also shows that the LOS probability obtained in (54) has a close match to that in the 3GPP model. It should be noted that even though our pathloss model is based on Manhattan distance, Euclidean distance is still a widely adopted metric in understanding urban cellular system, since it is generally easier to measure and manipulate. We use the Euclidean distance based LOS probability to evaluate the Euclidean distance based pathloss model in [14] and also to verify MPLP street models by comparing to 3GPP Euclidean distance based LOS

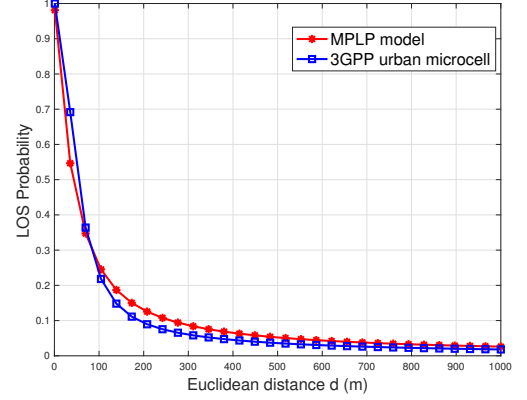


Fig. 10. Comparison of LOS probability under MPLP model and the expression in 3GPP microcellular model.

models.

### B. BS association probability

In this section, we analyze the BS association under the Manhattan distance based pathloss model in MPLP. We start with the analysis of association probability. Given the CDF of the associated link path gain in Section III-B, we derive the probability the receiver is associated with a LOS BS.

**Corollary 1.** *The probability  $\chi_T$  that the receiver is associated with a typical BS is*

$$\begin{aligned} \chi_T &\stackrel{(a)}{=} \mathbb{E}_u \left\{ \mathbb{P} \left( u_C < u \mid u_T = u \right) \right\} = \mathbb{E}_{u_T} \left\{ \mathbb{P} \left( u_C < u_T \right) \right\} \\ &\stackrel{(b)}{=} \int_0^\infty \exp \left( -\gamma_C \lambda_B^{\frac{\alpha_L}{\alpha_N}} u^{-\frac{1}{\alpha_N}} - \gamma_T \lambda_B u^{-\frac{1}{\alpha_L}} \right) \frac{\gamma_T \lambda_B}{\alpha_L} u^{-\frac{1}{\alpha_L}-1} du \\ &\stackrel{(c)}{=} \gamma_T \int_0^\infty \exp \left( -\gamma_C x^{\frac{\alpha_L}{\alpha_N}} - \gamma_T x \right) dx, \end{aligned} \quad (56)$$

where (a) is conditioned of maximum path gain of typical BSs is  $u$ , (b) is based on the CDF of the maximum path gain of typical/cross BSs, (c) follows by change of variables  $x = \lambda_B u^{-\frac{1}{\alpha_L}}$ .

Since the argument of the second exponential function in (56) is the multiplication of  $\lambda_S$  and an additional attenuation of corner loss, the argument inside tends to be very small. Similar to the approximation in Section IV, we approximate the association probability by

$$\begin{aligned} \chi_T^{\text{Approx}} &= \int_0^\infty \exp(-\mu) \left( 1 - \frac{\zeta_2}{\gamma_T^{\frac{\alpha_L}{\alpha_N}}} \lambda_S \mu^{\frac{\alpha_L}{\alpha_N}} \right) d\mu \\ &= 1 - \frac{2^{\frac{\alpha_L}{\alpha_N}+1} \gamma_C}{\gamma_T^{\frac{\alpha_L}{\alpha_N}}} \left[ \text{sinc} \left( \frac{\alpha_L}{\alpha_N} \right) \right]^{-1} \lambda_S, \end{aligned} \quad (57)$$

where  $\text{sinc}(x) = \frac{\sin \pi x}{\pi x}$ . Because the sinc function monotonously decreases with  $x$  ( $0 < x < 1$ ), the association probability with a typical BS decreases with  $\alpha_L$ , which is shown in Fig. 11. Different from  $\alpha_N$  which only impacts on the

NLOS BS pathloss, the LOS pathloss exponent  $\alpha_L$  is involved in both the calculation of typical/cross BS pathloss. The decrease of LOS association probability with larger  $\alpha_L$  implies that the LOS link pathloss is more sensitive to the changing pathloss exponents. Also, it is intuitive that the increase of  $\alpha_N$  enhances the association probability since it further attenuates the transmit signal from cross street BSs. It should be noted that it is meaningful to examine the interplay between the coverage probability and these exponents values, since the pathloss exponent in reality is not fixed (we extract two reasonable parameters for the ease of analysis in this paper), but is a random variable varying from streets to streets [27]. The interplay of pathloss exponents and LOS probability sheds light on the different BS association behaviors on different streets in an urban area.

In addition, from (57) there is a linear scaling law of LOS association probability with the intensity of cross streets in Fig. 11. Also, it should be noted that with the corner shadowing loss, even in an extremely dense street network, e.g.,  $\lambda_S = 0.1$ , the association probability with typical BSs  $\chi_T$  is still greater than 0.8. Only when in the case with no shadowing loss, the association probability  $\chi_T$  decreases significantly the street intensity  $\lambda_S$ . The above association probability analysis illuminates another important observation that considering shadowing loss at a reasonable value, cross BSs play a very minor role in BS association under the Manhattan distance based microcellular pathloss model. Similar effects on coverage probability have been demonstrated in Section III-C.

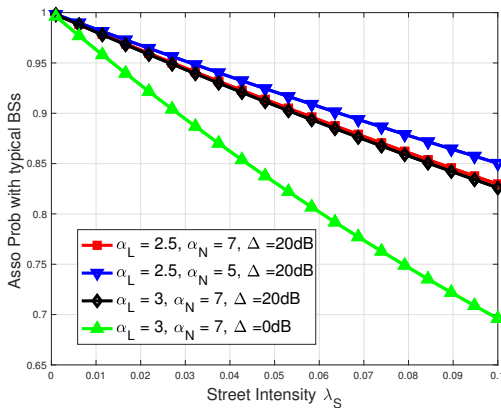


Fig. 11. Illustration of the exact and approximate propagation links for different kinds of BSs.

Hence, we can make the following conclusions about the BS association. First, the BS association probability is independent of the BS intensities. Second, the association probability decreases linearly with the intensity of the cross streets. Also, LOS association is less likely when the LOS pathloss exponent  $\alpha_L$  increases.

## VI. COMPARISON OF DIFFERENT PATHLOSS & STREET MODELS

In this section, first, we fit the pathloss data of the Manhattan distance based pathloss model to different Euclidean

distance based models and get the parameters for Euclidean distance pathloss models. Then we compare the coverage probability and the ergodic rate of the Manhattan distance based pathloss model adopted in this paper and the Euclidean distance pathloss models. Second, we compare the ergodic rate  $\mathcal{R} = \mathbb{E}\{\log_2(1 + \text{SINR})\}$  under different street modelings, respectively MPLP model in this paper, the fixed grid model and realistic street data of Chicago city obtained from OpenStreetMap [29].

### A. Pathloss models comparison

We compare our model with two different Euclidean distance based pathloss models. The first model computes the pathloss directly by Euclidean distance  $d$ , where  $\text{PL}_{\text{dB}}(d) = 10\tilde{\alpha} \log_{10} d + \Delta_1$ ,  $\tilde{\alpha}$  is the pathloss exponent, and  $\Delta_1$  is the offset for straight-line linear regression of the Euclidean pathloss model. In [14], a key parameter for characterizing coverage in mmWave wireless networks is the distance dependent blockage probability, which has been analyzed in Section V-A. In the urban microcell downlink scenario, we define it as  $p_B(d) = 1 - p_{\text{LOS}}(d)$  and apply different pathloss exponents  $\tilde{\alpha}_L$  and  $\tilde{\alpha}_N$  for unblocked (LOS) and blocked (NLOS) links. The pathloss is calculated by  $\text{PL}_{\text{dB}}(d) = (1 - \mathbb{I}(p_B(d))) (10\tilde{\alpha}_L \log_{10} d + \Delta_2^L) + \mathbb{I}(p_B(d)) (10\tilde{\alpha}_N \log_{10} d + \Delta_2^N)$ , where  $\mathbb{I}(x)$  is the Bernoulli function with parameter  $x$ ,  $\Delta_2^L$  and  $\Delta_2^N$  are respectively the offsets for LOS and NLOS pathloss formulas. The simulation parameters used in this Section are summarized in Table I.

TABLE I  
SIMULATION PARAMETERS

PARAMETERS	VALUES
LOS Pathloss Exponent $\alpha_L$	2.5
NLOS Pathloss Exponent $\alpha_N$	7
Corner Loss $\Delta$	20dB
Intensity of Street $\lambda_S$	0.01
Intensity of BS $\lambda_B$	0.01

The fitting parameters are given in Table II. Based on the linear regression results in Table II, we compare the coverage probability and ergodic rate of these three models in Fig. 12 and Fig. 13. It is shown that the three models show significant difference in coverage probability and ergodic rate. This motivates us to do further theoretical analysis in our proposed model.

TABLE II  
LINEAR REGRESSION RESULTS

PARAMETERS	VALUES
Fit Parameter $\tilde{\alpha}$ in Euclidean Model	11.8
Fit Parameter $\Delta_1$ in Euclidean Model	-19dB
Fit Parameter $\tilde{\alpha}_N$ in Model of [14]	11.1
Fit Parameter $\Delta_2^N$ in Model of [14]	5dB
Fit Parameter $\tilde{\alpha}_L$ in Model of [14]	2.5
Fit Parameter $\Delta_2^L$ in Model of [14]	0dB

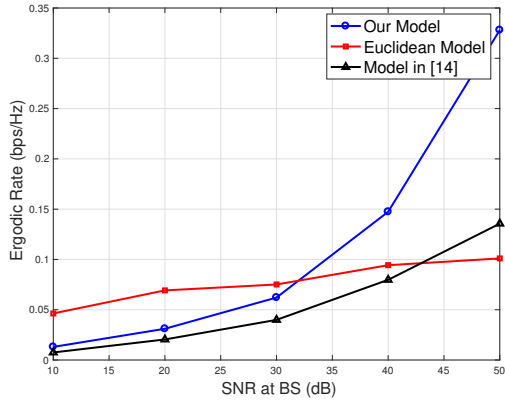


Fig. 12. Comparison of the three pathloss models in terms of ergodic rate against the transmit SNR at BS.

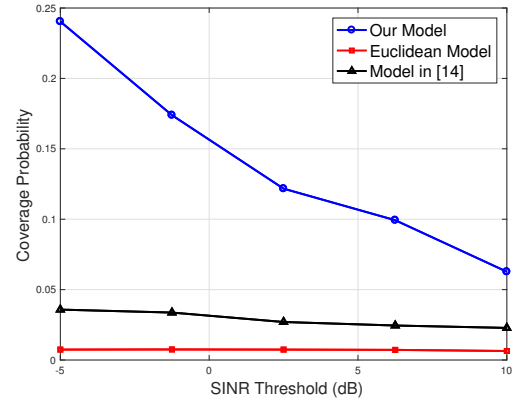


Fig. 13. Comparison of the three pathloss models in terms of coverage probability against the SINR Threshold.

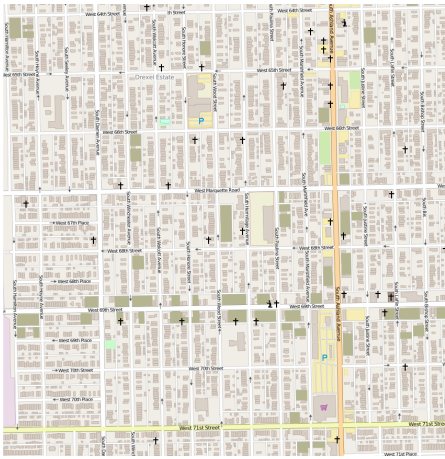


Fig. 14. A snapshot of downtown Chicago streets from OpenStreetMap (Latitude: 41.762°N- 41.78°N, Longitude: -87.678°W - -87.658°W), with a size of 1.659×2.002 (km<sup>2</sup>).

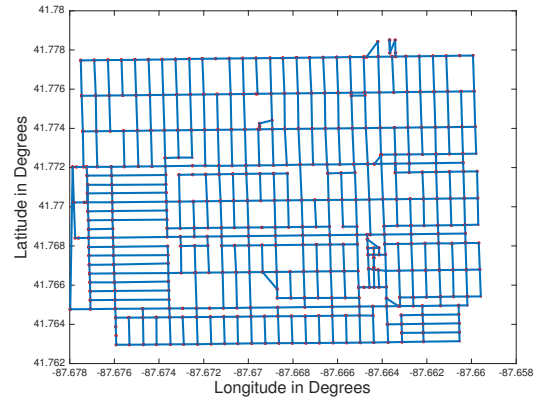


Fig. 15. Streets abstracted from OpenStreetMap by QGIS. The red points are the intersections obtained from QGIS and the plot is obtained by lining up the intersections that has one common intersected street.

### B. Street models comparison

In this section, we compare the ergodic rate under three different street models. The MPLP street modeling in this paper, fixed grid model (fixed spacing between streets) and realistic street deployments in downtown Chicago. The raw street data is obtained *OpenStreetMap* powered by open source software and [29], [30]. The simulated area is a part of downtown of Chicago given in Fig. 14, and map exported to Matlab is plotted in Fig. 15.

The comparison of the ergodic rate under the three models is given in Fig. 16. From this figure, it is clear that the capacities are very close under these different street models, which nearly coincide. Combining the analysis of LOS probability in Section V-A, we are able to justify the accurateness of urban street modeling by MPLP. Also, compared to the fixed grid model, which is widely adopted in Manhattan-kind urban street modeling, the MPLP model has the merit of yielding fairly tractable analysis. Its accuracy and tractability hence make MPLP a strong candidate in modeling urban street networks.

## VII. CONCLUSION

In this paper, we proposed a mathematical framework to model a Manhattan-type microcellular network under the urban mmWave communication system by stochastic geometry. We first analyze the distribution of the path gain to the BS. We then derive an exact yet concise expression of the coverage probability. The LOS interference from the BSs on the same street as the serving BS is the dominating factor in determining the coverage probability, while BSs on cross and parallel streets have insignificant effects. It was shown that in the ultra-dense network where intensity of BSs grows large, the network is interference-limited and the coverage probability approaches an asymptotic value. Also, the coverage probability scales linearly with the intensity of streets, and displays an interesting interplay with the BS intensity: i) when BS deployment is dense, coverage probability decreases with street intensity; ii) when BS intensity is small, the coverage probability increases with street intensity. This implies that the system does not work efficiently when both BS and street intensities are very large. Therefore, there is no need to deploy many BSs in an already dense urban street environment. In addition, we showed that the LOS BSs still dominate the



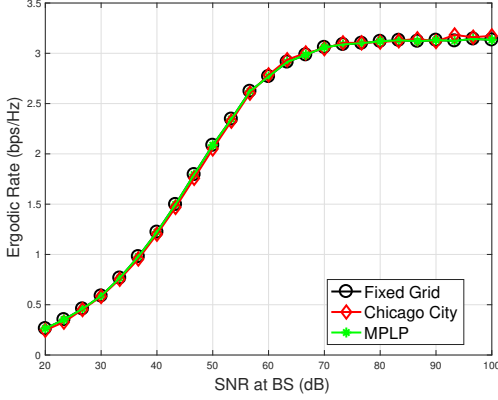


Fig. 16. Comparison of ergodic rate among MPLP street modeling, fixed grid model and real streets obtained from Chicago city.

performance of the whole system, from the perspective of both BS association, as well as coverage. Also, it was shown that the probability that a receiver associates to LOS BSs is independent of the intensity of BSs, while it decreases linearly with the intensity of streets. Further, the LOS link is more sensitive to the change of propagation environments, i.e., the change of LOS pathloss exponent. We also derived LOS probability and compared it with 3GPP microcellular model. The good match between LOS probability under MPLP in this paper and 3GPP realistic urban microcellular model justifies the validity of applying MPLP in street modeling. Finally, we numerically compared the ergodic rates under MPLP, fixed spacing and a realistic Chicago street model. It was shown that the ergodic rate under these street models match well, reinforcing the validity of MPLP as a realistic yet accurate urban street model.

#### APPENDIX A PROOF OF LEMMA 1

Denote the PPP of the BSs on typical street with gain  $G$  as  $\Psi_T$  and with gain  $g$  as  $\bar{\Psi}_T$ , then the CDF of the largest channel gain from BSs on the typical street is

$$\begin{aligned}
 F_{u_T}(u) &= \mathbb{P} \left( \max \left\{ \max_{x \in \Psi_T} Gx^{-\alpha_L}, \max_{x \in \bar{\Psi}_T} gx^{-\alpha_L} \right\} < u \right) \\
 &\stackrel{(a)}{=} \mathbb{P} \left( \max_{x \in \Psi_T} Gx^{-\alpha_L} < u \right) \mathbb{P} \left( \max_{x \in \bar{\Psi}_T} gx^{-\alpha_L} < u \right) \\
 &= \mathbb{P} \left( \min_{x \in \Psi_T} x > G^{\frac{1}{\alpha_L}} u^{-\frac{1}{\alpha_L}} \right) \mathbb{P} \left( \min_{x \in \bar{\Psi}_T} x > g^{\frac{1}{\alpha_L}} u^{-\frac{1}{\alpha_L}} \right) \\
 &\stackrel{(b)}{=} \exp \left( -2 \left( \lambda_b G^{\frac{1}{\alpha_L}} + \bar{\lambda}_b g^{\frac{1}{\alpha_L}} \right) u^{-\frac{1}{\alpha_L}} \right) \\
 &\stackrel{(c)}{=} \exp \left( -2\lambda_B \left( p_T G^{\frac{1}{\alpha_L}} + (1-p_T) g^{\frac{1}{\alpha_L}} \right) u^{-\frac{1}{\alpha_L}} \right), \tag{58}
 \end{aligned}$$

where (a) and (c) follows from the independent thinning of BSs on the typical street of BSs with different antenna gains, (b) is based on the distribution of closest distance to one fixed point of one-dimensional PPP with intensity  $\lambda$ ,  $\min\{x\} \sim \exp(2\lambda)$ .

Similarly, for the CDF of the largest channel gain from the BSs on the cross streets, we consider the BSs with antenna gain as  $G$  first as

$$\begin{aligned}
 F_{u_C}(u) &= \mathbb{E} \left[ \prod_{(x_C, y_C) \in \Phi_C} \mathbb{P} \left( x_C^{-\alpha_N} y_C^{-\alpha_L} cG < u \right) \right] \\
 &= \mathbb{E} \left[ \prod_{(x_C, y_C) \in \Phi_C} \mathbb{P} \left( x_C^{-\alpha_N} \min(y_C)^{-\alpha_L} cG < u \right) \right] \\
 &\stackrel{(a)}{=} \mathbb{E} \left[ \prod_{x_C} \exp \left( -2\lambda_b x_C^{-\frac{\alpha_N}{\alpha_L}} (cG)^{\frac{1}{\alpha_L}} u^{-\frac{1}{\alpha_L}} \right) \right] \\
 &\stackrel{(b)}{=} \exp \left( -2\lambda_S \int_0^\infty 1 - \exp \left( -2\lambda_b x^{-\frac{\alpha_N}{\alpha_L}} (cG)^{\frac{1}{\alpha_L}} u^{-\frac{1}{\alpha_L}} \right) du \right) \\
 &= \exp \left( -2\lambda_S (2\lambda_B)^{\frac{\alpha_L}{\alpha_N}} p_T^{\frac{\alpha_L}{\alpha_N}} (cG)^{\frac{1}{\alpha_N}} u^{-\frac{1}{\alpha_N}} \Gamma \left( 1 - \frac{\alpha_L}{\alpha_N} \right) \right), \tag{59}
 \end{aligned}$$

where (a) follows the void probability of the PPP and (b) is based on the probability generating functional (PGFL). Hence, by the independent thinning, the proof is concluded.

Here, we provide a lower bound of the CDF of the associated link path gain, where the lower bound is achieved when we assume the strongest path has beamforming gain  $G$ . Also, from the demonstration in Section II-E, the strongest path is always via the cross street closest to the receiver. Based on this assumption, the lower bound of the CDF can be derived as

$$\begin{aligned}
 F_{u_P}(u) &\geq \mathbb{P} \left( \bigcap_{(x_P, y_P, z_P) \in \Phi_P} x_P^{-\alpha_N} y_P^{-\alpha_N} z_P^{-\alpha_L} c^2 G < u \right) \\
 &= \mathbb{E}_{x_P} \left\{ \prod_{y_P} \exp \left( -2\lambda_b u^{-\frac{1}{\alpha_L}} c^{\frac{2}{\alpha_L}} G^{\frac{1}{\alpha_L}} x_P^{-\frac{\alpha_N}{\alpha_L}} y_P^{-\frac{\alpha_N}{\alpha_L}} \right) \right\} \\
 &= \mathbb{E}_{x_P} \left\{ \exp \left( -2\lambda_S (2\lambda_B)^{\frac{\alpha_L}{\alpha_N}} c^{\frac{2}{\alpha_N}} G^{\frac{1}{\alpha_L}} u^{-\frac{1}{\alpha_N}} \Gamma \left( 1 - \frac{\alpha_L}{\alpha_N} \right) x_P^{-1} \right) \right\} \\
 &= \int_0^\infty 2\lambda_S \exp \left( -\gamma_{P1} \lambda_B^{\frac{\alpha_L}{\alpha_N}} x^{-1} - 2\lambda_S x \right) dx \\
 &= 2\lambda_S \sqrt{\frac{2\gamma_P \lambda_B^{\frac{\alpha_L}{\alpha_N}} u^{-\frac{1}{\alpha_N}}}{\lambda_S}} K_1 \left( 2\sqrt{2\gamma_P \lambda_S \lambda_B^{\frac{\alpha_L}{\alpha_N}} u^{-\frac{1}{\alpha_N}}} \right). \tag{60}
 \end{aligned}$$

The last equation follows from [36], which concludes the proof.

#### APPENDIX B PROOF OF THEOREM 1

We respectively give the LT of the three kinds of interferers  $\phi_T$ ,  $\phi_C$  and  $\phi_P$ . The LT of the typical BS interference  $\mathcal{L}_{I_{\phi_T}}(s)$  with beamforming gain as  $G$  can be given by

$$\begin{aligned}
 \mathcal{L}_{I_{\phi_T}}(s) &= \mathbb{E} \left[ \exp \left( -s \sum_{x_T \in \Phi_T} h x_T^{-\alpha_L} \right) \right] \\
 &= \exp \left( -2\lambda_b \int_{\left(\frac{s}{G}\right)^{-\frac{1}{\alpha_L}}}^\infty \mathbb{E} \left( 1 - \exp(-s G h x_T^{-\alpha_L}) \right) \right)
 \end{aligned}$$

$$= \exp \left( -2\lambda_b \int_{\left(\frac{u}{G}\right)^{\frac{1}{\alpha_L}}}^{\infty} \frac{1}{1+s^{-1}G^{-1}x_T^{\alpha_L}} dx_T \right). \quad (61)$$

Then plugging in  $s = Tv^{-1}$  and by change of variables  $\mu = x \left(\frac{u}{G}\right)^{\frac{1}{\alpha_L}}$  the result can be simplified by

$$\mathcal{L}_{I_{\phi_T}}(s) = \exp \left( -2\lambda_b u^{-\frac{1}{\alpha_L}} G^{\frac{1}{\alpha_L}} \int_1^{\infty} \frac{1}{1+T^{-1}\mu^{\alpha_L}} d\mu \right). \quad (62)$$

The LT of the NLOS interferers on cross streets with beamforming gain  $G$  follows the similar proof in Appendix A and proof of  $I_{\phi_T}$ , which is

$$\begin{aligned} \mathcal{L}_{I_{\phi_C}}(s) &= \mathbb{E} \left[ \exp \left( - \sum_{(x_C, y_C) \in \Phi_C} s h x_C^{-\alpha_N} y_C^{-\alpha_L} cG \right) \right] \\ &= \mathbb{E} \left[ \prod_{x_C} \exp \left( -2\lambda_b x_C^{-\frac{\alpha_N}{\alpha_L}} u^{-\frac{1}{\alpha_L}} (cG)^{\frac{1}{\alpha_L}} \varrho(T) d\mu \right) \right] \\ &= \exp \left( -2\lambda_S \left( 2\lambda_b (cG)^{\frac{1}{\alpha_L}} \varrho(T) \right)^{\frac{\alpha_L}{\alpha_N}} \Gamma \left( 1 - \frac{\alpha_L}{\alpha_N} \right) u^{-\frac{1}{\alpha_N}} \right). \end{aligned} \quad (63)$$

For BSs with beamforming gain  $g$ , the results can be obtained by changing  $G$  in (62) and (63). The LT of parallel BS is also similar and we omit it here.

## REFERENCES

- [1] Y. Wang, K. Venugopal, A. F. Molisch, and R. W. Heath Jr., "Analysis of urban millimeter wave microcellular networks," in *Proc. IEEE VTC fall*, pp. 1–5, Sept. 2016.
- [2] J. Miller, "Vehicle-to-vehicle-to-infrastructure (V2V2I) intelligent transportation system architecture," in *Proc. Intelligent Vehicles Symposium*, pp. 715–720, IEEE, 2008.
- [3] P. Belanovic, D. Valerio, A. Paier, T. Zemen, F. Ricciato, and C. F. Mecklenbrauker, "On wireless links for vehicle-to-infrastructure communications," *IEEE Trans. Veh. Technol.*, vol. 59, no. 1, pp. 269–282, 2010.
- [4] J. Gozalvez, M. Sepulcre, and R. Bauza, "IEEE 802.11p vehicle to infrastructure communications in urban environments," *IEEE Commun. Mag.*, vol. 50, pp. 176–183, May 2012.
- [5] Z. Pi and F. Khan, "An introduction to millimeter-wave mobile broadband systems," *IEEE Commun. Mag.*, vol. 49, no. 6, pp. 101–107, 2011.
- [6] T. S. Rappaport, S. Sun, R. Mayzus, H. Zhao, Y. Azar, K. Wang, G. N. Wong, J. K. Schulz, M. Samimi, and F. Gutierrez, "Millimeter wave mobile communications for 5G cellular: It will work!," *IEEE access*, vol. 1, pp. 335–349, 2013.
- [7] T. S. Rappaport, R. W. Heath Jr, R. C. Daniels, and J. N. Murdock, *Millimeter wave wireless communications*. Pearson Education, 2014.
- [8] J. Choi, N. Gonzalez-Prelcic, R. Daniels, C. R. Bhat, and R. W. Heath Jr, "Millimeter wave vehicular communication to support massive automotive sensing," *arXiv preprint arXiv:1602.06456*, 2016.
- [9] H. T. Cheng, H. Shan, and W. Zhuang, "Infotainment and road safety service support in vehicular networking: From a communication perspective," *Mechanical Systems and Signal Processing*, vol. 25, no. 6, pp. 2020–2038, 2011.
- [10] A. V. Alejos, M. G. Sanchez, and I. Cuinas, "Measurement and analysis of propagation mechanisms at 40 GHz: Viability of site shielding forced by obstacles," *IEEE Trans. Veh. Technol.*, vol. 57, pp. 3369–3380, Nov 2008.
- [11] V. Va, T. Shimizu, G. Bansal, and R. W. Heath Jr, "Millimeter wave vehicular communications: A survey," *Foundations and Trends® in Networking*, vol. 10, no. 1, 2016.
- [12] Y. Niu, Y. Li, D. Jin, L. Su, and A. V. Vasilakos, "A survey of millimeter wave (mmWave) communications for 5G: Opportunities and challenges," *arxiv.org*, pp. 1–17, 2015.
- [13] J. G. Andrews, F. Baccelli, and R. K. Ganti, "A tractable approach to coverage and rate in cellular networks," *IEEE Trans. Commun.*, vol. 59, no. 11, pp. 3122–3134, 2011.
- [14] T. Bai and R. W. Heath, "Coverage and rate analysis for millimeter-wave cellular networks," *IEEE Trans. Wireless Commun.*, vol. 14, no. 2, pp. 1100–1114, 2015.
- [15] F. Baccelli and X. Zhang, "A correlated shadowing model for urban wireless networks," in *Proc. IEEE Infocom*, pp. 801–809, IEEE, 2015.
- [16] J. G. Andrews, T. Bai, M. Kulkarni, A. Alkhateeb, A. Gupta, and R. W. Heath, "Modeling and analyzing millimeter wave cellular systems," *IEEE Trans. Commun.*, 2016.
- [17] H. Elshaer, M. N. Kulkarni, F. Boccardi, J. G. Andrews, and M. Dohler, "Downlink and uplink cell association with traditional macrocells and millimeter wave small cells," *IEEE Trans. Wireless Commun.*, vol. 15, no. 9, pp. 6244–6258, 2016.
- [18] M. Di Renzo, "Stochastic geometry modeling and analysis of multi-tier millimeter wave cellular networks," *IEEE Trans. Wireless Commun.*, vol. 14, no. 9, pp. 5038–5057, 2015.
- [19] T. Bai, R. Vaze, and R. W. Heath, "Analysis of blockage effects on urban cellular networks," *IEEE Trans. Wireless Commun.*, vol. 13, no. 9, pp. 5070–5083, 2014.
- [20] M. N. Kulkarni, S. Singh, and J. G. Andrews, "Coverage and rate trends in dense urban mmwave cellular networks," in *IEEE GLOBECOM*, pp. 3809–3814, IEEE, 2014.
- [21] J. Lee, X. Zhang, and F. Baccelli, "A 3-D spatial model for in-building wireless networks with correlated shadowing," *IEEE Trans. Wireless Commun.*, vol. 15, pp. 7778–7793, Nov 2016.
- [22] A. F. Molisch, A. Karttunen, R. Wang, C. U. Bas, S. Hur, J. Park, and J. Zhang, "Millimeter-wave channels in urban environments," in *Proc. 10th European Conference on Antennas and Propagation (EuCAP)*, pp. 1–5, IEEE, 2016.
- [23] G. R. MacCartney, J. Zhang, S. Nie, and T. S. Rappaport, "Path loss models for 5g millimeter wave propagation channels in urban micro-cells," in *Global Communications Conference (GLOBECOM)*, 2013 IEEE, pp. 3948–3953, IEEE, 2013.
- [24] T. S. Rappaport, F. Gutierrez, E. Ben-Dor, J. N. Murdock, Y. Qiao, and J. I. Tamir, "Broadband millimeter-wave propagation measurements and models using adaptive-beam antennas for outdoor urban cellular communications," *IEEE Trans. Antennas and Propagation*, vol. 61, no. 4, pp. 1850–1859, 2013.
- [25] V. Nurmela, A. Karttunen, A. Roivainen, L. Raschkowski, T. Imai, J. Jarvelainen, J. Medbo, J. Vihriala, J. Meinila, K. Haneda, *et al.*, "Metis channel models," *FP7 METIS, Deliverable D*, vol. 1, 2015.
- [26] K. Haneda, L. Tian, Y. Zheng, H. Asplund, J. Li, Y. Wang, D. Steer, C. Li, T. Balercia, S. Lee, *et al.*, "5G 3GPP-like channel models for outdoor urban microcellular and macrocellular environments," *arXiv preprint arXiv:1602.07533*, 2016.
- [27] A. F. Molisch, A. Karttunen, S. Hur, J. Park, and J. Zhang, "Spatially consistent pathloss modeling for millimeter-wave channels in urban environments," in *Proc. 10th European Conference on Antennas and Propagation (EuCAP)*, pp. 1–5, 2016.
- [28] K. Venugopal, M. C. Valenti, and R. W. Heath, "Device-to-device millimeter wave communications: Interference, coverage, rate, and finite topologies," *IEEE Trans. Wireless Commun.*, vol. 15, pp. 6175–6188, Sept 2016.
- [29] <http://www.openstreetmap.org/>.
- [30] M. Haklay and P. Weber, "Openstreetmap: User-generated street maps," *IEEE Pervasive Computing*, vol. 7, no. 4, pp. 12–18, 2008.
- [31] F. Ramm, J. Topf, and S. Chilton, *OpenStreetMap: using and enhancing the free map of the world*. UIT Cambridge Cambridge, 2011.
- [32] D. QGIS, "Quantum GIS geographic information system," *Open Source Geospatial Foundation Project*, vol. 45, 2011.
- [33] F. Baccelli and B. Blaszczyzyn, *Stochastic geometry and wireless networks: Theory*, vol. 1. Now Publishers Inc, 2009.
- [34] S. N. Chiu, D. Stoyan, W. S. Kendall, and J. Mecke, *Stochastic geometry and its applications*. John Wiley & Sons, 2013.
- [35] J. E. Berg, "A recursive method for street microcell path loss calculations," in *Proc. PIMRC*, vol. 1, pp. 140–143 vol.1, Sep 1995.
- [36] I. S. Gradshteyn and I. M. Ryzhik, *Table of integrals, series, and products*. Academic press, 2014.
- [37] <http://dlmf.nist.gov/10.30#SS1.info>.
- [38] M. Haenggi, *Stochastic geometry for wireless networks*. Cambridge University Press, 2012.
- [39] E. U. T. R. Access, "Further advancements for E-UTRA physical layer aspects," *3GPP Technical Specification TR*, vol. 36, p. V2, 2010.